Eur. Phys. J. D **37**, 409–415 (2006)
DOI: 10.1140/epjd/e2005-00319-x

THE EUROPEAN PHYSICAL JOURNAL D

Structural deformation, melting point and lattice parameter studies of size selected silver clusters

I. Shyjumon[1,a], M. Gopinadhan[1], O. Ivanova[1], M. Quaas[2], H. Wulff[2], C.A. Helm[1], and R. Hippler[1]

[1] Institut für Physik, Ernst-Moritz-Arndt-Universität Greifswald, Domstraße 10a, 17489 Greifswald, Germany
[2] Institut für Chemie und Biochemie, Ernst-Moritz-Arndt-Universität Greifswald, Soldmannstraße 16, 17489 Greifswald, Germany

Received 9 September 2005 / Received in final form 3 November 2005
Published online 29 November 2005 –

Abstract. Silver clusters have been produced by magnetron sputtering in a gas aggregation nanocluster source. Clusters are size selected using a quadrupole mass filter (3–8 nm) or by varying the aggregation tube length (9–20 nm) of the nanocluster source. Mass selected clusters are deposited on a Si(100) substrate at different bias voltages and are characterized by atomic force microscopy. We observe a significant flattening of clusters on the surface due to the increase of impact energy as a result of increasing substrate bias voltage. The behavior of lattice parameters for size selected clusters are investigated by X-ray diffraction. All measured lattice constants exhibit a tensile strain; it is found that the lattice constant slightly increases with increasing cluster size up to a size of 12 nm and then decreases. The melting temperature of deposited clusters is found to be size-dependent and significantly lower than for bulk material, in agreement with theoretical considerations.

PACS. 36.40.-c Atomic and molecular clusters – 36.40.Wa Charged clusters – 36.40.Qv Stability and fragmentation of clusters – 61.46.+w Nanoscale materials: clusters, nanoparticles, nanotubes, and nanocrystals

1 Introduction

The physics and chemistry of nanoscale systems have advanced significantly over the last 10 years and there are attractive prospects for translating the original scientific developments into a new generation of high technology materials and processes [1–3]. Clusters are intermediate states of matter in the course of transition from the gaseous state to a condensed state. A cluster as a system of bound atoms constitutes a physical object that is of interest both from the fundamental and applied standpoints. Use of clusters in the form of cluster beams is convenient for both the generation and application of clusters [4]. Fundamental physical interest of clusters arises due to their reduced size [5]. Cluster-surface interaction studies draw interests due to both the fundamental aspects of the mechanisms involved in the interaction [6], and their potential industrial applications such as nanoelectronics, heterogeneous catalysis etc. Also the interaction between energetic clusters and surfaces is of growing scientific interest because of their potential importance for such applications as surface metallization, surface cleaning, catalysis, precision machining, and cluster fusion [7–10]. Ionized cluster beam deposition has recently received a great deal of attention as promising method for synthesizing high-quality thin films at low temperatures [8–10]. In the process of nanoclusters deposition on a substrate, the particles are distributed randomly on the surface and there is local fluctuation in the deposition rate. This results in the development of surface roughness. However, an activation energy in the form of higher substrate temperature or energetic impact of clusters with the substrate may be needed to assist efficient surface diffusion and thus a uniform and high quality nanocluster film is obtained [11].

Here we report an investigation of size selected Ag cluster ion deposition. Size selection was carried out by varying the cluster forming chamber (aggregation tube) length and/or with the help of a QMF 200 mass filter [12]. Cluster formation growth and cluster-substrate interaction are in the center of interest. The flattening of mass selected and charge separated Ag clusters on the substrate by applying a substrate bias voltage is observed. The size effect of nanoparticles on the lattice constant is described in many articles and the authors found decreasing as well as increasing lattice constants with size [13–16]. It seems that the size effect on the lattice constants strongly depends on the deposition conditions (*particle-surface* interaction) and the nanostructure evolution during cluster growth (*inter-particle* interaction). We investigated the influence of cluster sizes on lattice parameters and on cluster melting points by characterizing samples with different cluster size, obtained by varying the aggregation tube length.

[a] e-mail: shyju@physik.uni-greifswald.de

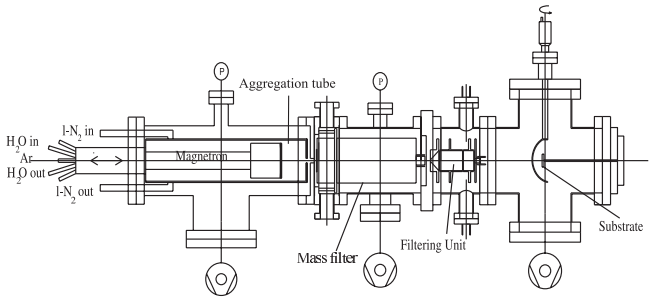

Fig. 1. Experimental set-up (schematic).

2 Experimental set-up

Our studies evolve along the following lines,

- formation of metal (Ag) clusters inside a NC 200 nanoclusters source [17];
- size selection of the produced clusters either by varying the cluster forming chamber (aggregation tube) length or by the employment of a QMF 200 mass filter followed by charge separation;
- deposition of clusters on a Si(100) substrate by varying the time of deposition and the energy between substrate and the cluster, i.e., by applying a substrate bias voltage V_s;
- characterization of the deposited clusters using atomic force microscopy (AFM) and grazing incidence X-ray diffraction (GIXD).

Figure 1 shows the schematic sketch of the experimental set-up, that is equipped with a NC 200 nanocluster source (Oxford Applied Research) inside a vacuum chamber. The target atoms are sputtered out by a direct current (dc) magnetron sputtering based on a concept developed by Haberland et al. [18–20]. Clusters form by the attachment of free atoms and coagulation process [4,17] inside the liquid nitrogen (L–N_2) cooled aggregation tube of variable length. These clusters flow together with the carrying gas (Ar) through a variable orifice with a typical diameter of 3 mm. Then these clusters can be selected by mass in a QMF 200 mass filter [12], followed by charge separation by an extraction unit. The extraction unit consists of a set of electric plates, applying a proper polarity to these plates enables us to select only one type of charged clusters (we selected only positive charged clusters for this study by applying an extraction voltage of –700 V). Finally these clusters are deposited on a Si(100) substrate kept at a distance of about 53 cm from the exit of the magnetron chamber.

AFM and GIXD techniques are used to characterize these films. Atomic force microscopy (AFM) is done using Digital nanoscope IIIa in tapping mode [21,22], with high resolution Hi'res DP15 tips (MikroMasch). *Sewing tip approach* was used in order to avoid tip damage. Set point value was chosen to be ∼0.9 V, with target amplitude 1 V to reduce tip artifacts. Scanning Probe Imaging Processor (SPIP) along with Nioprobe tip characterizer was used to get the upper bound tip radius ($R_T \sim 4$ nm) of the HI'Res tips.

Grazing incidence diffractometry (GIXD) in off-specular reflectivity geometry is performed using a $\theta - \theta$ diffractometer (XRD3000, Seifert with Cu–Kα radiation) [23]. An integrated high temperature chamber (Bühler HDK2.4) allows in-situ measurements at temperatures up to 1000 °C. In the traditional Warren-Averbach plot, the linear part of the graph $\ln F(L)/L$ versus L allows for domain size determination. Qualitatively, an increase in peak width indicates a decrease in domain size. For a quantitative analysis, one has also to describe the peak profile by Stokes Fourier series. The Fourier coefficients $F(L)$ of the physical line profile contain information about particle size [24].

3 Results and discussion

In this section we present the results obtained from cluster films prepared at various experimental conditions to get information on

(a) time effect of cluster growth (different surface coverage);
(b) cluster flattening on impact on a substrate (clusters are mass selected by QMF 200 mass filter) by changing the substrate bias voltages (different impact energies/force);
(c) lattice parameters and melting point of size selected clusters.

The initial energy of deposited clusters estimated from the deflection of cluster beam in an electric field is of the order of 0.1 eV/atom.

3.1 Time effect of cluster growth without size selection

Samples are prepared with Ag clusters at different deposition times keeping the aggregation region at a temperature of 148 K. In this case the whole cluster band corresponding to an aggregation tube length of 15 cm is allowed to pass to the substrate without any further size selection. The surface coverage and the extracted mean height is shown in Figure 2.

Under the present conditions, the sputtering yield for Ag is 1.4 [25,26]; it leads to a high density of sputtered Ag atoms in the magnetron chamber, and conversely of clusters and results in a high surface coverage at longer deposition time. A closer inspection of the AFM picture (Fig. 3) of Ag clusters deposited for 15 s shows both isolated and aggregated clusters on Si(100) wafer. Statistical analysis of Figure 3 reveals that about 40% of the clusters are completely isolated, most clusters are very close to each other forming 2-dimensional aggregates. Very few aggregates (<3%) show growth in the third dimension (cluster on top of each other). This shows the formation of bigger nanoparticles as a result of coagulation of two or more neighbouring clusters because of the surface diffusion as well as the possibility of clusters landing on top of each other far before the first layer is completed. For longer deposition times even more clusters get aggregated.

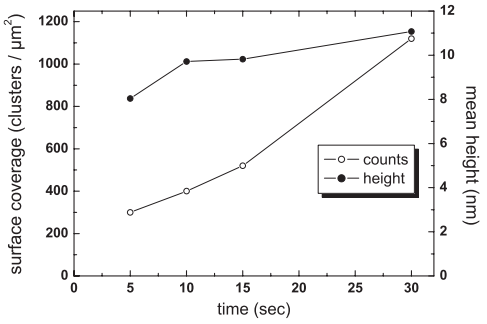

Fig. 2. The surface coverage of deposited clusters (○) and the extracted mean heights (●) versus deposition time without size selection ($T = 148$ K).

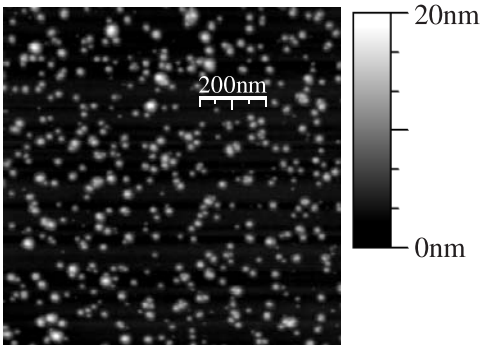

Fig. 3. Aggregation of clusters due to coagulation of neighbouring clusters (time of deposition 15 s, cluster forming chamber length 15 cm and temperature 148 K).

3.2 Size selection without and with mass filter

The size selection using the QMF 200 mass filter results in a small size distribution whereas a simple variation of the tube length results a rather broad distribution. The highest mass that can be selected using the QMF 200 mass filter [12] is $\sim 2 \times 10^6$ amu (average size $\sim$8 nm). Figure 4 shows the height histograms with lognormal fit from the AFM measurements of samples prepared without and with mass filter for the same tube length of 16 cm (deposition time for the samples without and with mass filter is 25 s and 55 s, respectively. Aggregated clusters were omitted in the height analysis).

3.3 Mass selection of clusters using QMF 200 mass filter

In QMF 200 quadrupole mass filter clusters can be selected according to their mass to charge ratio by the quadrupole electric field so that only ions of a defined mass M will be transmitted [12]. The motion of ions inside the quadrupole is described by Mathieu equation [27]. The mass selection is controlled by the frequency f (kHz) and the amplitude of ac voltage V_{ac} (in Volts),

$$M = 7 \times 10^7 \, k \, \frac{V_{ac}}{f^2 d^2} \qquad (1)$$

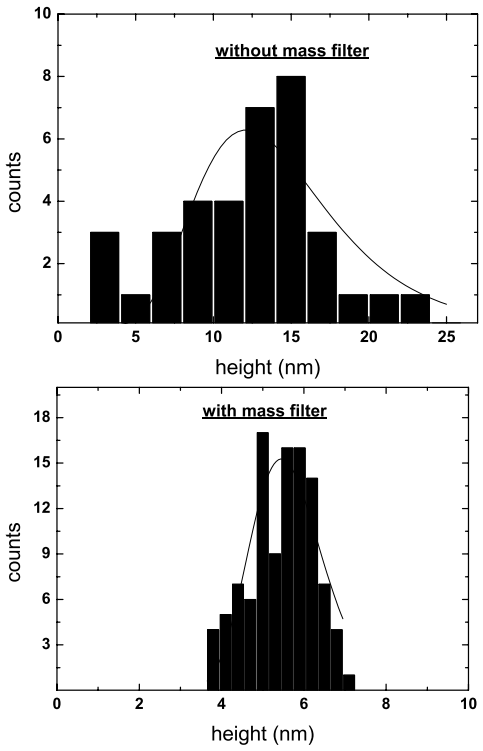

Fig. 4. Comparison of height histograms without and with mass filter.

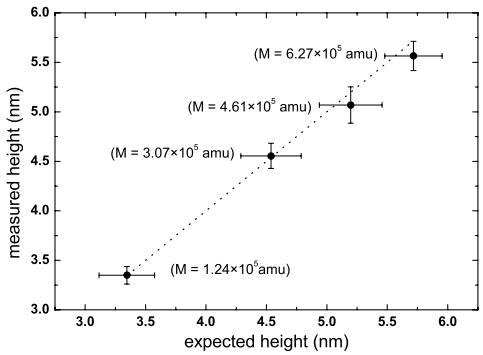

Fig. 5. Height comparison for mass selected clusters by the mass filter, the dotted line corresponds to measured height equal to expected height.

where M is the cluster mass in atomic mass units (amu), $d = 25.4$ mm is the rod diameter, and k is a correction factor of order unity.

Ag clusters with different cluster mass, selected by QMF 200 by adjusting the frequency f and voltage V_{ac} are deposited on a Si(100) substrate. These samples are characterized by AFM in order to determine the height of the clusters. Figure 5 shows a comparison between the expected cluster height (calculated from the selected mass) and the AFM measured cluster height which is in perfect agreement. For the comparison, a correction factor $k = 1.23$ is used.

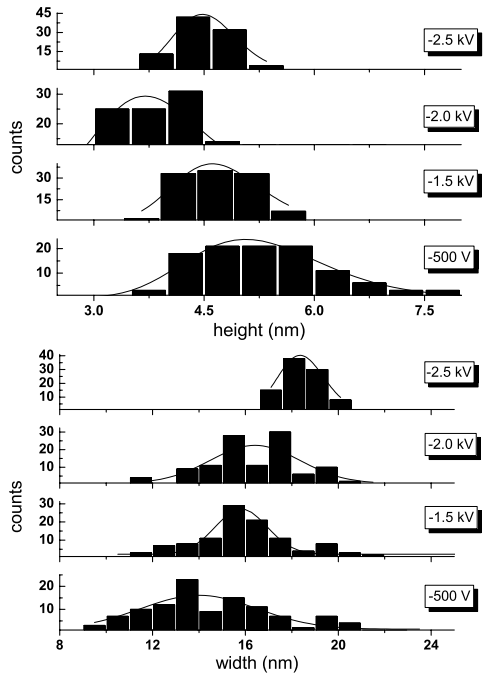

Fig. 6. Height and width histograms at different substrate bias voltages. $t = 240$ s, $T = 198$ K.

3.3.1 Flattening of mass selected clusters versus substrate bias voltage

In order to investigate the cluster-surface interaction in some detail, we have performed experiments at different substrate bias voltages V_s.

Ag clusters have been produced inside the NC 200 nanocluster source [17], by operating the magnetron at a power of 113 W and keeping the aggregation region at a temperature of 198 K. Clusters with mean mass $M = 2.3 \times 10^5$ amu (average size ∼4.1 nm, $N \sim 2131$ atoms) are mass-selected inside the QMF 200 mass filter. Finally these clusters are deposited on a Si(100) substrate, placed at a distance of 230 mm from the exit of mass filter, at substrate bias voltage ranging from –500 V to –2500 V. Samples deposited for 240 s with different substrate bias voltages are analyzed by AFM. The corresponding height and width histograms with lognormal fits for different substrate voltages are shown (Fig. 6). The measured AFM image is a convolution of the tip geometry and the geometry of the clusters. In order to determine the real width from the measured width one has to find an approximate value for the deconvolution factor. For calibration we used spherical Au colloidal particles (Sigma Aldrich) with diameter ∼4 nm. The AFM measured average height of the Au particles is ∼3.5 nm and the corresponding full width at half maximum is ∼12.5 nm, giving a correction factor to the tip geometry ∼9 nm for the AFM measured width of the clusters. Assuming a spherical geometry to the tip apex one can obtain a simple expression to evaluate the real width of the Au nanoparticles [28],

$$W = 4\sqrt{R_p R_T}\,, \qquad (2)$$

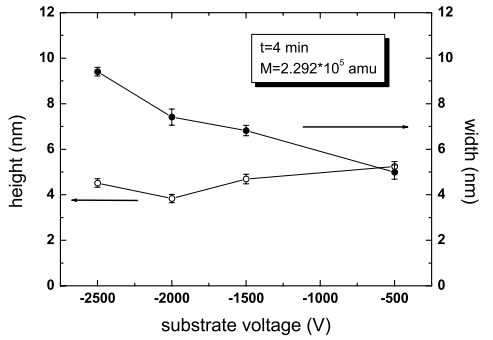

Fig. 7. Relation of height (○) and width (●) of clusters with substrate voltage after deconvoluting for the tip geometry.

with R_p the real particle radius, R_T the tip radius and W the AFM measured full width at half maximum. With the Hi'res tips ($R_T \sim 4$ nm) we obtained $R_P \sim 2$ nm from the above geometrical equation. The average height (∼3.5 nm) measured with Hi'res tips shows that the Au nanoparticles are spherical and the geometrical equation is valid. So without loss of generality we have used 9 nm as the deconvolution factor for the AFM measured lateral width of the Ag clusters. Figure 7 shows the extracted relation of mean cluster height (vertical) and width (horizontal) for the applied accelerating (bias) voltage at the substrate. The results infer that the cluster mean height (vertical) somewhat decreases with increasing substrate voltage, whereas the width (horizontal) of the clusters increases with increasing substrate voltage. This points towards a flattening of the clusters on the surface due to higher attraction or stress. Some discrepancies remain, as the extracted cluster volume as function of substrate voltage is not constant, however the exact shape of the clusters on surface has yet to be found.

3.3.2 Explanation for flattening of clusters

The flattening of clusters on a surface can be qualitatively explained in terms of cluster-surface collision processes. Several studies have been done in this field [6,29–31]. In general cluster-surface collisions can be described as low energy, medium energy or high energy processes. One of the important parameters that decides the mechanism of cluster interaction with the surface is the impact energy along with the nature of cluster as well as substrate material. In our case, clusters with mass ∼10^5 amu are having an initial energy $E_0/N \sim 0.1$ eV/atom, and $N \sim 2 \times 10^3$ atoms. At the point of impact the energy/atom increases to $E/N = E_0/N + eV_s/N$, due to the substrate bias applied. Energetic cluster impact on surfaces which may lead to pinning, implantation or flattening are studied by several authors [6,32,33]. Since our clusters have a medium impact energy (0.1 to 1 eV/atom) we expect mainly plastic deformation and fragmentation from the whole listed collision processes [6], that ends up in the spreading or flattening of the clusters on the surface.

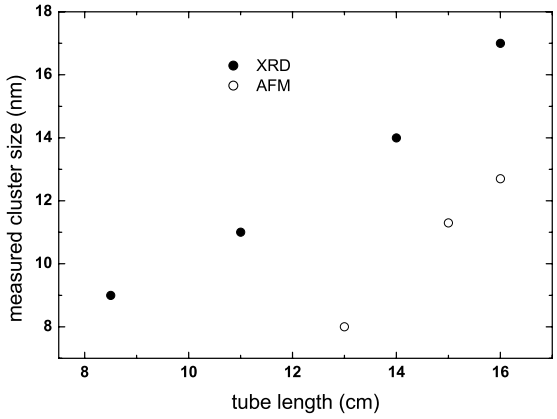

Fig. 8. Cluster sizes measured by GIXD (•) and by AFM (○) at different aggregation tube lengths.

3.4 Size effect on melting point and lattice parameters of Ag clusters

The length of the aggregation tube (cluster forming chamber) in the magnetron chamber of NC 200 nanocluster source can be changed with the help of an external rotary drive. By increasing the length (thereby the volume) of the aggregation tube the residence time of the growing clusters increases, which helps the clusters to grow to bigger sizes.

3.4.1 Cluster size determination by AFM & GIXD

Samples with different cluster size are prepared by adjusting the aggregation tube length. Figure 8 shows the relation between measured average cluster size by grazing incidence X-ray diffractrometry (GIXD) and by AFM measurements.

There is a discrepancy between AFM and GIXD measurements for cluster size (Fig. 8), the reason is given by the broad size distribution. For AFM we only take into account the isolated clusters where as in GIXD the whole area is investigated, so the aggregated clusters on surface are also included. In addition the very small clusters can not be seen with GIXD because of the small coherence length. Furthermore the samples investigated by GIXD are having a higher surface coverage, which may lead to cluster coalescence on the substrate surface.

3.4.2 Melting of clusters

Theoretical considerations about the size effect on the melting point suggest a depression of melting point for the measured clusters sizes. To collaborate the theory of melting and plastic deformation due to cluster-surface collision we carried out annealing experiments using in-situ high-temperature GIXD. The X-ray pattern of deposited Ag-clusters shows characteristic peaks of fcc-Ag. Ag(111) reflection is the most intensive peak in the X-ray pattern of randomly oriented polycrystalline Ag.

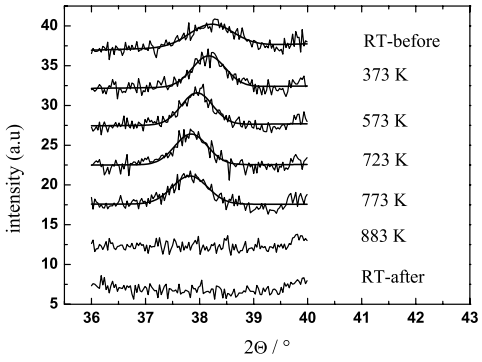

Fig. 9. Examples of in-situ GIXD measurements by annealing sample with cluster size of 15 nm.

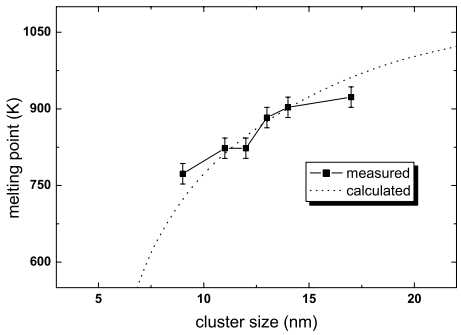

Fig. 10. The dependence of cluster melting point on size, the dotted line is calculated from equation (3).

Samples were prepared with different domain (cluster) sizes by varying the aggregation tube length. To get reasonable coverage the time of deposition was 15 min (cluster multilayers), at a temperature inside the aggregation tube of 173 K and a substrate voltage of –1.5 kV. The measurement details are,

(i) X-ray diffractometry at grazing incidence: $\omega = 0.5^{\circ}$, exit angle $2\Theta = 36^{\circ}...46^{\circ}$ at $P = 5 \times 10^{-3}$ mbar;
(ii) heating: in-situ measurements from 373 K–973 K with 30 min holding time before each measurement. For lower temperatures we used a step size of 100 K, reducing the step size to 10 K near the melting point;
(iii) room temperature measurements before and after annealing.

Figure 9 shows diffractometry measurements of the Ag(111) reflection at different temperatures. While heating up the samples a peak shift caused by thermal expansion can be observed. At a certain temperature no more crystalline silver was found, indicating cluster melting. On cooling no crystalline Ag is found and after annealing there is no trace of Ag, that means practically an evaporation takes place.

The melting of the samples appears in the temperature range between 853 K and 883 K depending on cluster size (Fig. 10), whereas the melting point of bulk silver is 1233 K [34]. The cluster sizes are obtained from GIXD measurements. The very small melting point of samples is because of the small grain size. The larger the influence of

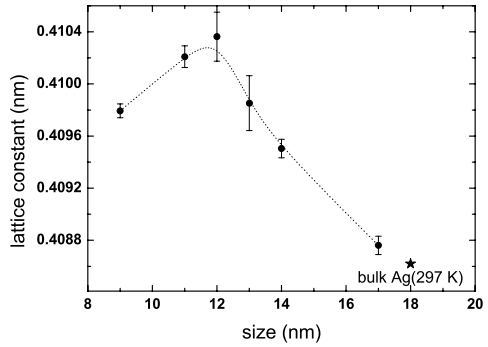

Fig. 11. Lattice constant as a function of cluster size.

surface atoms compared to the internal atoms, the smaller will be the melting point. The decrease of the melting point ΔT for small crystallites of radius r can be calculated from the Gibbs-Thomson equation [35];

$$\Delta T = \frac{4\sigma M T_{bulk}}{\Delta H_m r \rho} \tag{3}$$

with $\sigma = 1.02$ J/m^2 the surface energy, $M = 107.9$ g/mol the molar mass, $T_{bulk} = 1233$ K the melting point of the bulk material, $\Delta H_m = 11.3$ kJ/mol the melting enthalpy and $\rho = 10.5$ g/cm^3 the density of the material.

Our experimental results confirm the theoretical considerations. The good agreement between theoretically calculated and the experimentally observed melting points also demonstrates the capability of GIXD technique as powerful tool for cluster size measurements.

3.4.3 Change in lattice constant with decreasing nanoparticle size

AFM measurements exhibit a characteristic deformation of the deposited clusters in dependence on the impact energy. The deformation of the clusters occurs via two distinct processes: elastic (reversible) and plastic (irreversible) deformation.

Nanoparticles of Ag were prepared as described above and deposited on a Si(100) wafer that is biased by a substrate voltage $V_s = -1.5$ kV, the deposition time was 15 min. The lattice constants for samples with different cluster sizes were measured at room temperature in grazing incidence geometry. Figure 11 shows the lattice constant of Ag clusters as a function of cluster size.

The measured lattice constants change with Ag nanocluster sizes. Clusters from 9 to 12 nm size the lattice constant increases and then up to 17 nm the lattice constant converge to bulk silver, $a_0 = 0.4086$ nm [34]. For all investigated clusters we found strains due to residual tensile stresses. It is worth noticing that strain is the result of lattice disorders and structural disorder.

During the impact of the clusters on the substrate high temperatures and hence a local melting of the clusters are conceivable. Because of the distinct differences in thermal expansion coefficients of Si substrate and Ag a tensile stress within the clusters results. As described in Section 3.4.2 the melting temperature increases with increasing cluster size. Thus the influence of the local melting adjacent to the substrate will be reduced with increasing cluster size and the lattice constants should converge to the bulk value as observed for sizes larger than 12 nm.

The decreasing lattice constants of the clusters with diameters below 12 nm are not yet understood in detail. In the gas phase, it is well-known that average bond distances in small metal clusters (2–7 nm) are shorter than in bulk material, a feature which is accompanied by increased binding energies of the atoms in the small clusters compared to the bulk phase [36,37]. The bond length contraction becomes very pronounced for clusters consisting of only a few atoms. However, the volume constraints due to the cluster size increase lead to an increase in lattice size. The fact that we observe the maximum of the lattice distance at larger diameters (i.e., 12 nm) may be attributed to the tensile stresses the clusters experience on hitting the silicon surface.

4 Conclusions

Nanosized Ag clusters are produced inside a gas aggregation nanocluster source followed by the deposition on a Si(100) substrate. The effect of deposition time on the layer growth study infers that the cluster aggregation on surface starts far before the first layer is completed (around 10 s). Size selection of the clusters are done by using QMF 200 mass filter or by varying the aggregation tube length of nannocluster source. On impact on a biased surface the mass selected clusters suffer a deformation, leading to a more extended shape (more precisely getting flattened). The flattening of clusters on surface is directly proportional to the bias voltage. Results are presented for the lattice constant relation to individual domain (cluster) size, where the lattice constant increases at smaller domain (cluster) sizes but decreases after a size of 12 nm. Also found a proportional increase of cluster melting point with individual domain (cluster) size. The theoretically calculated values fit well with the measured melting points.

Part of this work was supported by the International Max-Planck-Research School (IMPRS) *Bounded Plasmas*. Financial support by the Deutsche Forschungsgemeinschaft through SFB/TR 24 *Fundamentals of Complex Plasmas* is gratefully acknowledged.

References

1. H. Gleiter, Nanostruct. Mater. **1**, 1 (1992)
2. P. Jensen et al., in *Nanostructure and nanocrystals*, edited by H.S. Nalwa (American Scientific Publishers, 2003)
3. B.M. Smirnov, I. Shyjumon, R. Hippler, Phys. Scripta (accepted, 2005)
4. B.M. Smirnov, Physics-Uspekhi. **46**, 589 (2003)
5. P. Jensen, Rev. Mod. Phys. **71**, 1695 (1999)

6. W. Harbich, in *Metal Clusters at Surfaces*, edited by K.H. Meiwes-Broer (Springer-Verlag, New York, 1997)
7. H. Hsieh, R.S. Averback, H. Sellers, C.P. Flynn, Phys. Rev B **45**, 4417 (1992)
8. J. Matsuo, E. Minami, M. Saito, N. Toyoda, H. Katsumata, I. Yamada, Eur. Phys. J. D **9**, 635 (1999)
9. Y. Fujiwara, I. Yamada, Nucl. Instr. Meth. B **206**, 875 (2003)
10. Y. Qiang, Y. Thurner, Th. Reiners, O. Rattunde, H. Haberland, Surf. Coat. Technol. **100-101**, 27 (1998)
11. M. Moseler, O. Rattunde, J. Nordiek, H. Haberland, Nucl. Instr. Meth. B **164**, 522 (2000)
12. Quadrupole mass filter - QMF 200, Oxford applied research, version 1.1
13. K. Sattler, *Handbook of thin film material*, edited by H.S. Nakawa (Academic press, 2002), Vol. 5, Chap. 2
14. P.A. Montano, W. Schulze, B. Tesche, G.K. Shenoy, T.I. Morrison, Phys. Rev. B **30**, 672 (1984)
15. J.M. Zuo, B.Q. Li, Phys. Rev. Lett. **88**, 255502 (2002)
16. F. Zhang, Siu-Wai Chan, J.E. Spanier, E. Apak, Q. Jin, R.D. Robinson, I.P. Herman, Appl. Phys. Lett. **80**, 127 (2002)
17. I. Shyjumon, M. Gopinadhan, C.A. Helm, B.M. Smirnov, R. Hippler, Thin Solid Films (accepted, 2005)
18. H. Haberland, *Clusters of atoms and molecules* (Springer-Verlag, New York, 1994)
19. H. Haberland, B. von Issendorff, Ji Yufeng, T. Kolar, Phys. Rev. Lett. **69**, 3212 (1992)
20. H. Haberland, M. Mall, M. Moseler, Y. Qiang, T. Reiners, Y. Thurner, J. Vac. Sci. Technol. A **12**, 2925 (1994)
21. G. Binnig, C.F. Quate, Ch. Gerber, Phys. Rev. Lett. **56**, 930 (1986)
22. C.A. Helm, P. Tippmann-Krayer, H. Möhwald, J. Als-Nielsen, K. Kjaer, Biophys. J. **60**, 1457 (1991)
23. H. Wulff, H. Steffen, in *Low temperature plasma physics*, edited by R. Hippler, S. Pfau, M. Schmidt, K.H. Schoenbach (Wiley-VCH, Berlin, 2001), Chap. 10
24. P. Klimanek, Mater. Sci. Forum **79-82**, 73 (1991)
25. D. Samsonov, J. Goree, J. Vac. Sci. Techn. A **17**, 2835 (1999)
26. D. Samsonov, J. Goree, Phys. Rev. E **59**, 1047 (1999)
27. *Atomic and molecular beam methods*, edited by G. Scoles (Oxford university press, Oxford, 1988), Vol. 1, Chap. 8
28. J. Vesenka, S. Manne, R. Giberson, T. Marsh, E. Henderson, Biophys. J. **65**, 992 (1993)
29. P. Jonk, R. Hector, F. Wittenberg, K.H. Meiwes-Broer, Nucl. Instr. Meth. Phys. Res. B. **80/81**, 818 (1993)
30. C.L. Cleveland, U. Landman, Science **257**, 355 (1992)
31. G. Betz, W. Husinsky, NIM B **122**, 311 (1997)
32. S.J. Carroll, S. Pratontep, M. Streun, R.E. Palmer, S. Hobday, R. Smith, J. Chem. Phys. **113**, 7723 (2000)
33. C. Xirouchaki, R.E. Palmer, Vaccum **66**, 167 (2002)
34. *Handbook of Chemistry and Physics*, 80th edn. (CRC-press, Cleveland, OH, 1999-2000)
35. K. Meyer, *Physikalisch chemische Kristallographie*, Deutscher Verlag für Grundstoffindustrie (Leipzig, 1968)
36. B. Richter, H. Kuhlenbeck, J.J. Freund, P. Bagus, Phys. Rev. Lett. **93**, 026805 (2004)
37. I. Lopez-Salido, D.C. Lim, Y.D. Kim, Surf. Sci. **588**, 6 (2005)